J Appl Electrochem (2011) 41:1349–1355
DOI 10.1007/s10800-011-0356-2

ORIGINAL PAPER

Synthesis of $LiFe_{0.4}Mn_{0.6-x}Ni_xPO_4/C$ by co-precipitation method and its electrochemical performances

Ke Du · Luo-Hu Zhang · Yan-Bing Cao · Hong-wei Guo · Zhong-Dong Peng · Guo-Rong Hu

Received: 21 June 2011 / Accepted: 14 September 2011 / Published online: 30 September 2011

Abstract $LiFe_{0.4}Mn_{0.6-x}Ni_xPO_4/C$($x = 0$, 0.05, 0.1, and 0.2) composite cathode materials for lithium ion batteries have been prepared by the co-precipitation method using oxalic acid as a precipitator. The structure and morphology of precursors and products have been investigated. Electrochemical tests demonstrate that $LiFe_{0.4}Mn_{0.55}Ni_{0.05}PO_4$ can deliver a specific capacity of 142 mAh g^{-1} at 0.1 *C*, and retains 133 mAh g^{-1} after 60 cycles. The rate performance of $LiFe_{0.4}Mn_{0.6}PO_4$ is obviously improved by doping Ni. The capacity of $LiFe_{0.4}Mn_{0.55}Ni_{0.05}PO_4$ at 2 *C* is 110 mAh g^{-1}.

Keywords Composite materials · Co-precipitation · X-ray scattering · Electrochemical properties

1 Introduction

Since the pioneering work of Goodenough and co-workers in 1997 [1], $LiFePO_4$ has now been recognized as one of the most promising cathode materials for large-scale Li-ion battery applications. The advantages of $LiFePO_4$ are the abundance of the raw materials, environmental friendliness, excellent cyclic stability, and high safety. At the same time, other materials based on the olivine structure like $LiMnPO_4$ have been intensively studied [2–4]. $LiMnPO_4$ has some advantages over its Fe counterpart. For example, the theoretical energy density of $LiMnPO_4$ is 697 Wh kg^{-1}, compared to 586 Wh kg^{-1} for $LiFePO_4$. The redox potential for the Mn^{3+}/Mn^{2+} couple is 4.1 V (vs. Li/Li^+) compared to 3.4 V (vs. Li/Li^+) for the Fe^{3+}/Fe^{2+} couple. However, $LiMnPO_4$ has lower electronic conductivity ($<10^{-10}$ S cm^{-1}) compared to $LiFePO_4$ (1.8×10^{-9} S cm^{-1}), which leads to poor rate performances [5]. A promising system is $LiMn_xFe_{1-x}PO_4$, which combines good electrochemical performances of $LiFePO_4$ with the high potential of $LiMnPO_4$ [6].

Padhi et al. [1] conducted systematic experiments on the electrochemical charge and discharge characteristics of $LiMn_xFe_{1-x}PO_4$ ($x = 0.25$, 0.50, 0.75, 1.0) and reported that the electrochemical capacity decreases rapidly at $x > 0.75$. Li et al. [7] also found that a comparatively high capacity was achieved with an average discharge voltage of 3.6 V at the Mn content of $y = 0.5$–0.75. And Yamada et al. [8–10] suggested $x = 0.6$ is an optimal choice. But recently, Martha et al. [11] have reported carbon-coated nano-particles of $LiMn_{0.8}Fe_{0.2}PO_4$ (C-$LiMn_{0.8}Fe_{0.2}PO_4$) prepared by solid state method could deliver a specific capacity of 100 mAh g^{-1} at 10 *C* when only $LiMn_{0.8}Fe_{0.2}PO_4$ was considered as the active material. And the study of Hu et al. [12] showed that the capacity of $LiMn_{0.9}Fe_{0.1}PO_4$ reached 130 mAh g^{-1} at 0.1 *C*.

However, the cycle ability of $LiMn_xFe_{1-x}PO_4$ is worse than that of $LiFePO_4$ due to the appearance of Jahn–Teller ion Mn^{3+} during the charge–discharge process [13–15]. In the case of $LiMn_2O_4$, doping other elements is an effective method to suppress the Jahn–Teller transition and many kinds of doping ions have been investigated [16–22]. In this study, nickel is chosen as a doping element considering its ability of forming a phosphate solid solution with $LiFePO_4$ and $LiMnPO_4$ [23]. In addition, this may form a layer of Li–Ni–PO_4 with high electronic conductivity on the surface of the olivine crystal [24, 25].

K. Du (✉) · L.-H. Zhang · Y.-B. Cao · H. Guo · Z.-D. Peng · G.-R. Hu
School of Metallurgical Science and Engineering, Central South University, Changsha 410083, People's Republic of China
e-mail: dukeben1976@yahoo.com

To insure the homogeneous distribution of transition metals, a mixed transition metal precursor in the form of oxalate has been prepared first in this article. Then the precursor reacts with other raw materials and the final phosphate solid solution is obtained.

2 Experimental

2.1 Sample preparation

Stoichiometric amounts of $FeSO_4{\cdot}7H_2O$, $MnSO_4{\cdot}H_2O$, and $NiSO_4{\cdot}6H_2O$ were dissolved in distilled water (cationic ratio of Fe:Mn:Ni is 4:6-*x*:*x*, $x = 0$, 0.05, 0.1, and 0.2), and the concentration of the total metal sulfate was 0.8 mol L^{-1}. The aqueous solution was precipitated by adding an $H_2C_2O_4$ solution of 0.6 mol L^{-1} with continuous stirring at 30 °C. Also a 0.3 mol L^{-1} NH_4OH solution was used to control the pH 4. A light-yellow mixed oxalate precipitate formed and then was filtrated, washed and dried at 80 °C for 24 h under active vacuum. Thereafter the dried powder was thoroughly mixed with Li_2CO_3 and $NH_4H_2PO_4$ (with the molar ratio of 2:1:2). At the same time, 6 wt% glucose was added as an organic additive. The mixture was ball-milled and then heated at 600 °C for 10 h in flowing Ar.

2.2 Sample characterization

The concentration of iron, manganese, and nickel of the synthesized materials were analyzed by using an inductively coupled plasma spectrometer (ICP, Optima 4300DV, PE Ltd.).

The size distribution of particles was measured by the laser diffraction method on a Malvern 2000 (Malvern).

X-ray diffraction (XRD) analysis was performed with a Philips X'Pert MPD (Philips) instrument to identify the crystal structure and the phase composition of the samples.

Scanning electronic microscopy (SEM) and Energy-dispersive spectrometry (EDS) were performed with a JSM-5600LV (JEOL) instrument to analyze the surface morphology, the size of particles and the map of different elements.

In order to determine the exact amount of carbon in the samples of $LiFe_{0.4}Mn_{0.6-x}Ni_xPO_4/C$($x = 0$, 0.05, 0.1, and 0.2), thermogravimetric analysis (TGA; Seiko 6300 TGADTA) was carried out in independent measurements. The samples were heated to 700 °C at a rate of 5 °C min^{-1}.

2.3 Electrochemical measurements

CR2025 coin-type cells were used as test vehicles. The positive electrodes were prepared by coating a mixture containing 80% active materials, 10% acetylene black, and 10% PVDF on Al current collector foil. The typical disk electrode contains active material of 4 mg cm^{-2} with a thickness of 80 μm. Metallic lithium foil was used as counter electrode, Cellgard 2300 was used as separator, and 1 M $LiPF_6$ dissolved in EC + DMC (1:1 in volume) was used as electrolyte. The test cells were assembled in a glove box with H_2O and O_2 were both below 1 ppm, and were tested between 3.0 and 4.5 V versus Li/Li^+ by using a Land CT 2001A battery test system (Land Co. China).

Cyclic-voltammetry (CV) measurements were carried out by using Model 2273A Electrochemical Instruments (PerkinElmer Co., USA) at room temperature. The sweeping rate was fixed at 0.05 mV s^{-1} in the voltage region from 2.5 to 4.8 V.

3 Results and discussion

The contents of Fe, Mn, and Ni in the four co-precipitated precursors $Fe_{0.4}Mn_{0.6-x}Ni_x(C_2O_4){\cdot}2H_2O$ are listed in Table 1. As shown in Table 1, the ratio of transition metal elements is very close to the targeted ratio for each precursor. The carbon contents in the four olivine samples determined by thermogravimetry are similar, around 3.5 wt%.

Figure 1 shows the XRD of the $Fe_{0.4}Mn_{0.6-x}Ni_x(C_2O_4){\cdot}2H_2O$ precursors with different x values ($x = 0$, 0.05, 0.1, and 0.2). All peak patterns match well the sets of XRD peaks from typical orthorhombic β-oxalate phases [26] for the four samples. The morphologies of the $Fe_{0.4}Mn_{0.6-x}Ni_x(C_2O_4){\cdot}2H_2O$ are shown in Fig. 2. Most of the precipitation particles have plate-like shape, which are more prominent in undoped and low content of Ni-doped samples. It seems that the existence of Ni^{2+} changes the precipitation circumstances because the dimension size of

Table 1 Mass percents of transition metals in mixed transition metal oxalates obtained from ICP-AES measurements

Samples	Fe% (wt)	Mn% (wt)	Ni% (wt)	Fe:Mn:Ni (mole ratio)	D_{50}/μm
$Fe_{0.4}Mn_{0.6}C_2O_4{\cdot}2H_2O$	13.17	17.39		0.43:0.57	40.34
$Fe_{0.4}Mn_{0.55}Ni_{0.05}C_2O_4{\cdot}2H_2O$	12.00	16.81	1.807	0.39:0.55:0.06	21.15
$Fe_{0.4}Mn_{0.5}Ni_{0.1}C_2O_4{\cdot}2H_2O$	12.35	14.62	3.52	0.4:0.49:0.11	13.07
$Fe_{0.4}Mn_{0.4}Ni_{0.2}C_2O_4{\cdot}2H_2O$	11.83	11.47	7.08	0.39:0.39:0.22	6.00

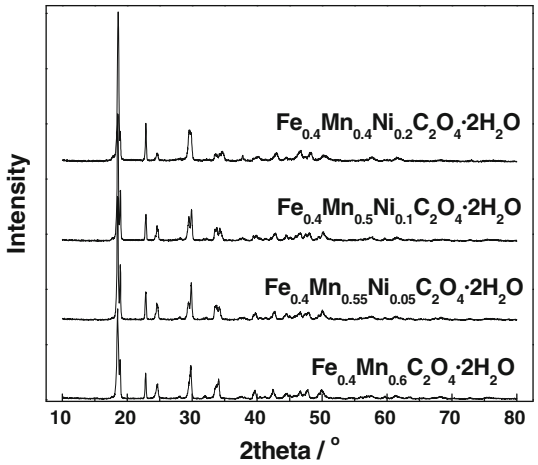

Fig. 1 XRD of precursor $Fe_{0.4}Mn_{0.6-x}Ni_x(C_2O_4){\cdot}2H_2O$($x = 0$, 0.05, 0.1, and 0.2)

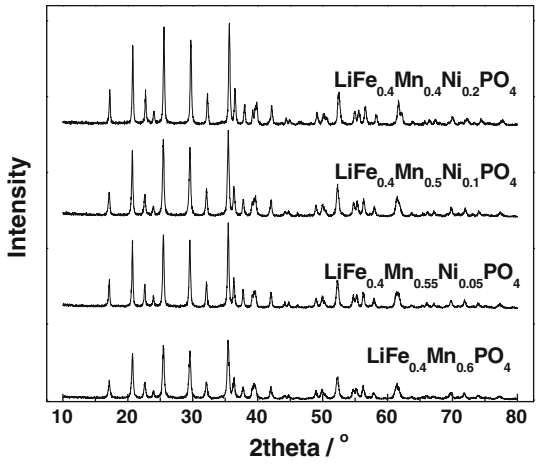

Fig. 3 XRD of $LiFe_{0.4}Mn_{0.6-x}Ni_xPO_4$ ($x = 0$, 0.05, 0.1, and 0.2)

particles decreases with the increase of Ni content. The sizes of the particles $Fe_{0.4}Mn_{0.6}(C_2O_4){\cdot}2H_2O$ are several times larger than that of $Fe_{0.4}Mn_{0.4}Ni_{0.2}(C_2O_4){\cdot}2H_2O$. The D_{50} values listed in Table 1 also show the large change of the particles sizes, from about 40 μm to about 6 μm.

The above four precursors are used as raw materials to synthesize $LiFe_{0.4}Mn_{0.6-x}Ni_xPO_4/C$($x = 0$, 0.05, 0.1, and 0.2), whose XRD patterns are showed in Fig. 3. It is observed that good crystalline products are obtained without second phases for all four samples. The crystalline parameters of the unit cell for each synthesized sample are calculated by the least squares method and listed in Table 2. For comparison, the reported lattice parameter of three end members, $LiFePO_4$, $LiMnPO_4$, and $LiNiPO_4$, are also listed [1, 27]. From Table 2, it tells clearly that the lattice parameter changes among the values of the end members. With the increase of the amount of Ni^{2+}, the lattice parameters reduce. It implies the substituted Ni^{2+} enters into the lattices to form a solid solution instead of a mixture.

Figure 4 shows the SEM of four $LiFe_{0.4}Mn_{0.6-x}Ni_xPO_4$ samples. All samples consist of agglomerated sub-micrometer particles and no obvious systematic change in the size of particles is detected by SEM observation. It seems that the large size differences of precursors caused by Ni doping disappear after sintering at high temperature.

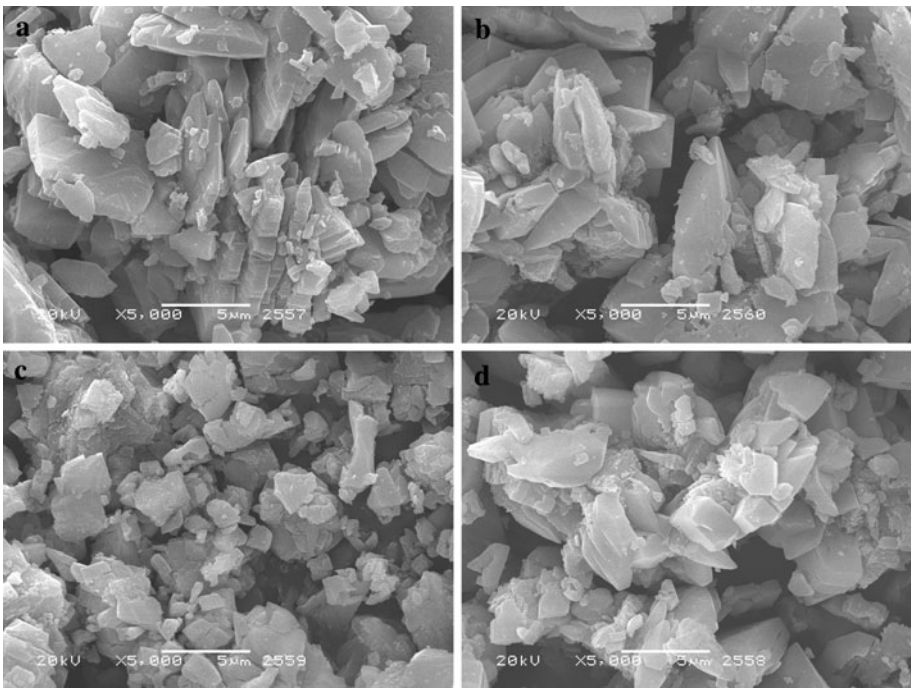

Fig. 2 SEM of precursor $Fe_{0.4}Mn_{0.6-x}Ni_x(C_2O_4){\cdot}2H_2O$ (**a** $x = 0$, **b** $x = 0.05$, **c** $x = 0.1$, and **d** $x = 0.2$)

Table 2 Cell parameters of $LiFe_{0.4}Mn_{0.6-x}Ni_xPO_4/C$($x = 0$, 0.05, 0.1, and 0.2)

Samples	Cell parameter/nm		
	a	*b*	*c*
$LiFe_{0.4}Mn_{0.6}PO_4$	0.6050	1.0367	0.4716
$LiFe_{0.4}Mn_{0.55}Ni_{0.05}PO_4$	0.6047	1.0367	0.4712
$LiFe_{0.4}Mn_{0.5}Ni_{0.1}PO_4$	0.6041	1.0364	0.4711
$LiFe_{0.4}Mn_{0.4}Ni_{0.2}PO_4$	0.6012	1.0305	0.4703
$LiFePO_4$ [1]	0.6008	1.0324	0.4694
$LiMnPO_4$ [2]	0.6108	1.0455	0.4750
$LiNiPO_4$ [19]	0.5854	1.0032	0.4677

The homogeneous distribution of Fe, Mn, and Ni ions on the surface of the particles for $LiFe_{0.4}Mn_{0.55}Ni_{0.05}PO_4$ is observed from EDS measurements as shown in Fig. 5. The other three samples have the similar homogeneity, which are not shown here. The results indicate that the synthesized phosphate solid solutions would be a single phase rather than a multiple one.

The results of the cycle characterizations of the Li/$LiFe_{0.4}Mn_{0.6-x}Ni_xPO_4$ cells at various rates from 0.1 to 2 *C* are presented in Fig. 6. The charge rate is fixed at 0.1 *C* to insure identical initial conditions for each discharge. It clearly demonstrates that the rate capability of the material is significantly improved by doping Ni. For example, in the case of an undoped sample, the cell delivers a high specific capacity of 148 mAh g^{-1} in the initial discharge at 0.1 *C*, but only 20 mAh g^{-1} at 2 *C*. It reduces rapidly with the increasing of the *C*-rate current. The $LiFe_{0.4}Mn_{0.55}Ni_{0.05}PO_4$ delivers a lower initial capacity of 142 mAh g^{-1} at 0.1 *C*, but maintains the discharge capacity of 139, 135, 127, and 110 mAh g^{-1} at 0.2, 0.5, 1, and 2 *C*, respectively. Samples with even higher Ni doping content, $LiFe_{0.4}Mn_{0.5}Ni_{0.1}PO_4$ and $LiFe_{0.4}Mn_{0.4}Ni_{0.2}PO_4$, have relatively low capacities at low rates, ca. 129 and 124 mAh g^{-1} at 0.1 *C*. But the rate capability is better than that of an undoped or a low doped sample. The ratios of the capacity at 2 *C* over that of 0.1 *C* are 12, 77, 81, and 84% for $LiFe_{0.4}Mn_{0.6-x}Ni_xPO_4$ with $x = 0$, 0.05, 0.1, and 0.2, respectively.

It seems that doping small amount of Ni can really improve the ion conductivity of $LiFe_{0.4}Mn_{0.6}PO_4$. However, too much Ni substitution for active Mn element, 16.7% and 33.3% for $LiFe_{0.4}Mn_{0.5}Ni_{0.1}PO_4$ and $LiFe_{0.4}Mn_{0.4}Ni_{0.2}PO_4$, should be responsible for the low capacity of these materials at a low rate. Moreover, doping Ni^{2+} may cause defects in the crystal, which accelerates Li^+ movement and improves the rate performance.

At the end of the rate performance tests, the discharged rate of the cells returns to 0.1 *C* after cycling at five different discharge rates. For $x = 0$, 0.05, 0.1, and 0.2, the discharge capacities decrease about 12, 9, 8, and 8 mAh g^{-1} after 55 cycles when compared to the capacities in the first cycle, respectively. The result means that substitution of Mn with Ni can improve the cycling ability of the material with limited effect.

Figure 7 shows the discharge curves of four samples at 0.1, 0.2, 0.5, 1, and 2 *C*. The charge rate is also fixed at

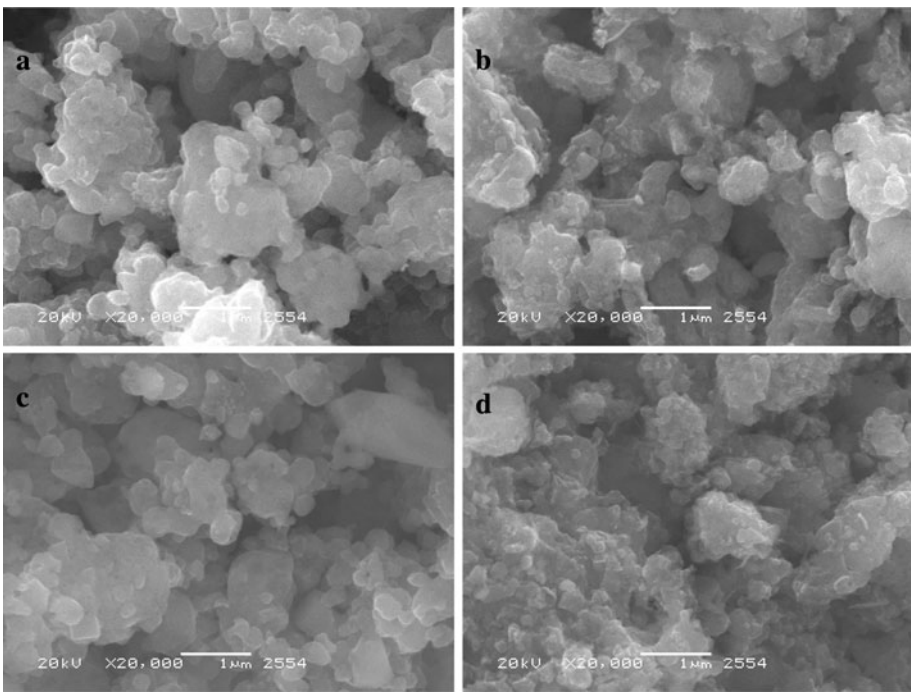

Fig. 4 SEM of precursor $LiFe_{0.4}Mn_{0.6-x}Ni_xPO_4$ (**a** $x = 0$, **b** $x = 0.05$, **c** $x = 0.1$, and **d** $x = 0.2$)

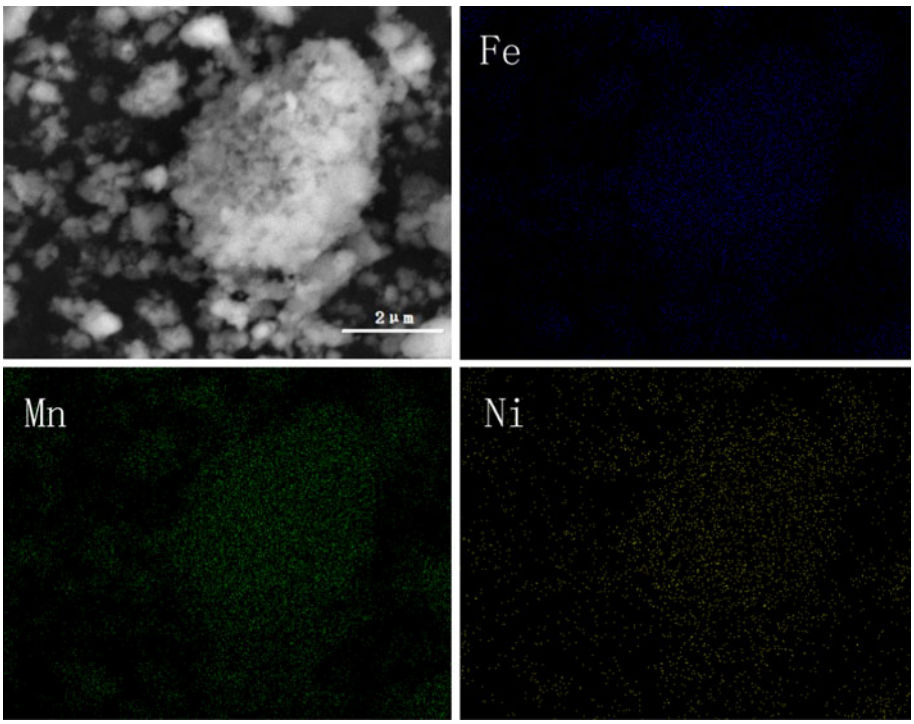

Fig. 5 The distribution of transition metals in $LiFe_{0.4}Mn_{0.55}Ni_{0.05}PO_4$ material observed by EDS

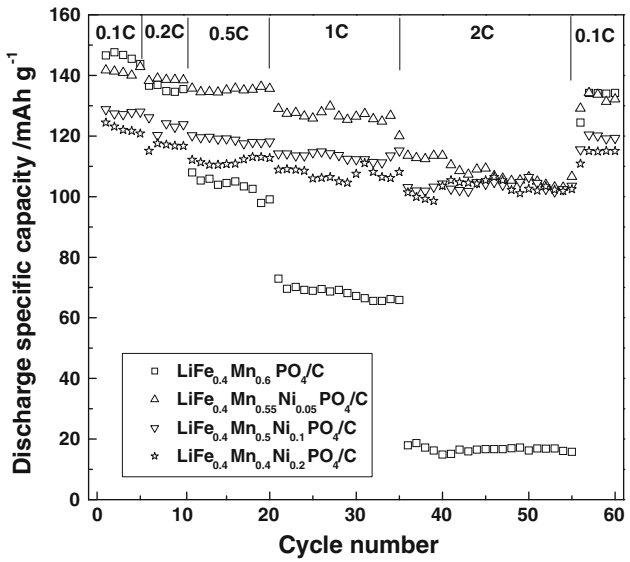

Fig. 6 Cyclability of $LiFe_{0.4}Mn_{0.6-x}Ni_xPO_4$ ($x = 0$, 0.05, 0.1, and 0.2)

0.1 *C*, which is not shown here. Two distinguished discharge plateaus are observed during low discharge rates, which represent the changes of $Mn^{3+} \rightarrow Mn^{2+}$ and $Fe^{3+} \rightarrow Fe^{2+}$. The main capacity fading of Ni-doped samples comes from the part corresponding to the redox reaction of $Mn^{3+} \rightarrow Mn^{2+}$. Considering the very high working voltage of $LiNiPO_4$ (above 5 V [28, 29]), Ni content is a kind of inert composition in this system. With the increase of the discharge rate, not only the discharge capacity decreases, but also the polarization becomes obvious. The increase in Ni content reduces the capacity fade and polarization by changing current density from 0.1 to 2 *C*. Because the carbon contents and particle sizes are similar in four samples, these results indicate that Ni play a significant role in improving high rate characteristics of $LiFe_{0.4}Mn_{0.6}PO_4$-based positive electrode materials. Similar effect has also been reported in the $LiMn_2O_4$-based materials [20–22].

To investigate the effect of doping Ni on the redox reaction of $LiFe_{0.4}Mn_{0.6}PO_4$, the CVs of four samples are depicted in Fig. 8. Two pairs of peaks correspond to two reaction processes: $Fe^{2+} \leftrightarrow Fe^{3+}$ (A and A′) and $Mn^{2+} \leftrightarrow Mn^{3+}$ (B and B′). With the increase of Ni, the peak area of Mn (B and B′) decreases obviously because the active Mn is substituted by the inactive Ni. And the less polarity of two reaction processes in doping samples is observed: the difference between the anodic and cathodic potential for $Fe^{2+} \leftrightarrow Fe^{3+}$ (A and A′) in $LiFe_{0.4}Mn_{0.6}PO_4$ is 0.36 V. There is only a difference of 0.30, 0.32, and 0.30 V for three doping samples. For $Mn^{2+} \leftrightarrow Mn^{3+}$ (B and B′), these differences are 0.44, 0.28, 0.34, and 0.26 V for the sample with doping amount of 0, 0.05, 0.1, and 0.2, respectively. So the presence of Ni in the solid solution of $LiFe_{0.4}Mn_{0.6}PO_4$ can alleviate polarity of the electrode reaction, which is in accordance with the results of rate experiments.

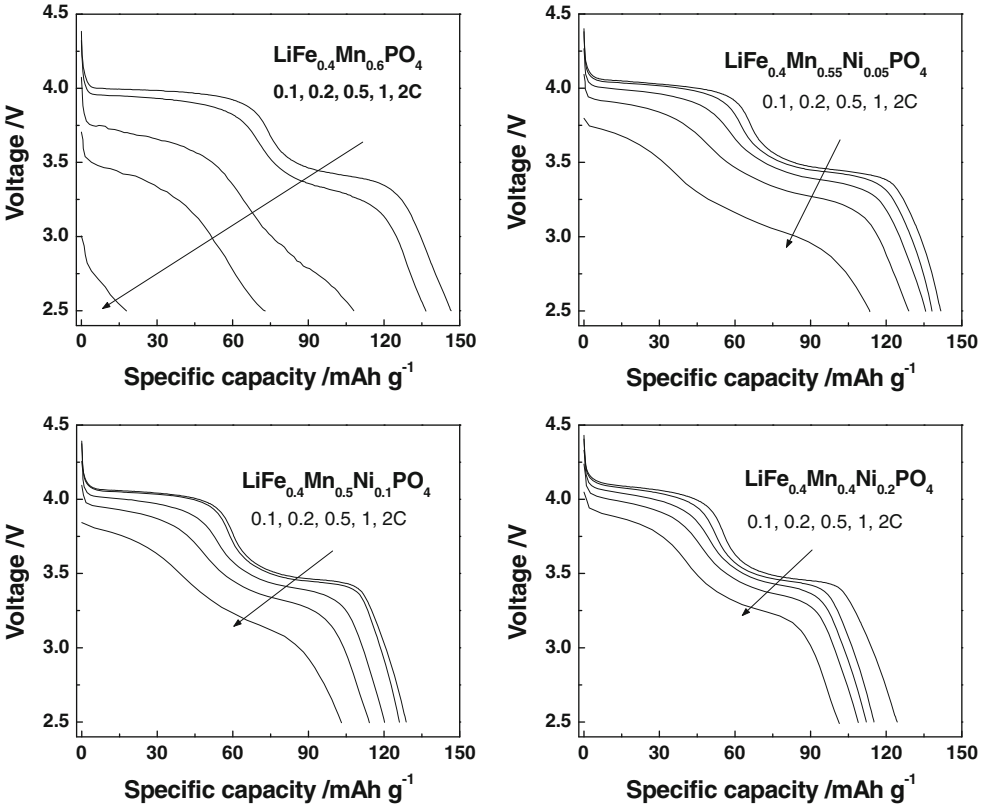

Fig. 7 Discharge curves of $LiFe_{0.4}Mn_{0.6-x}Ni_xPO_4$ ($x = 0$, 0.05, 0.1, and 0.2) at different rates

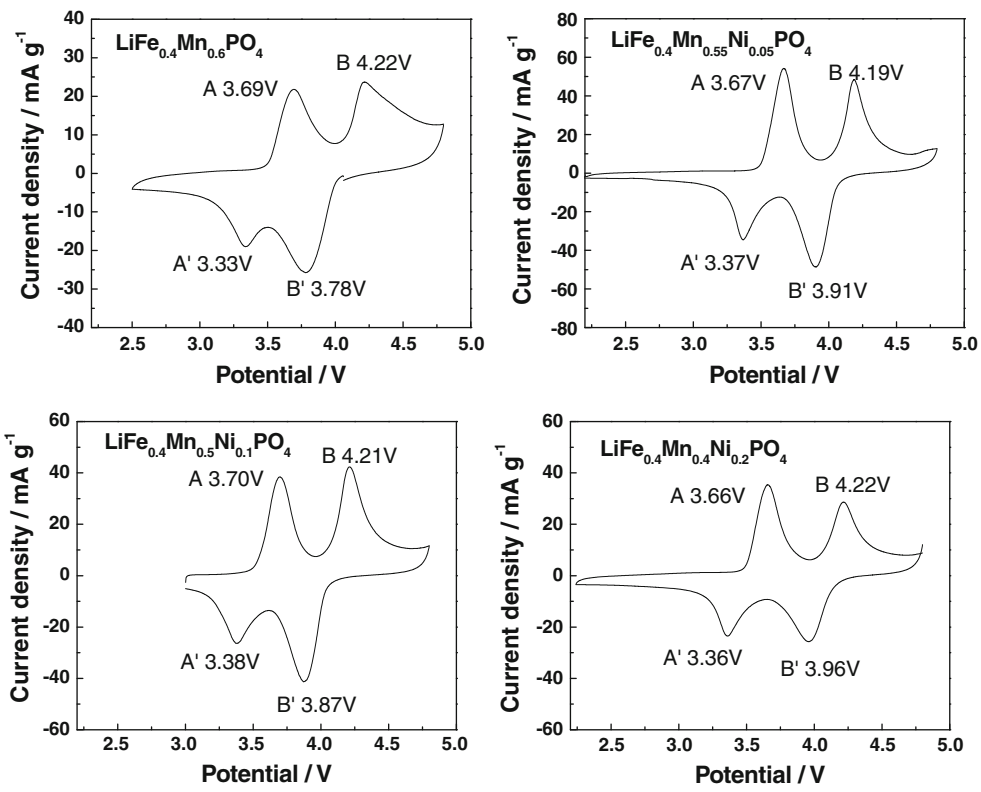

Fig. 8 Cyclic-voltammetries of $LiFe_{0.4}Mn_{0.6-x}Ni_xPO_4$ ($x = 0$, 0.05, 0.1, and 0.2)

4 Conclusion

Fe^{2+}, Mn^{2+}, and Ni^{2+} have been co-precipitated by $H_2C_2O_4$ at suitable conditions and a homogeneous $Fe_{0.4}Mn_{0.6-x}Ni_x(C_2O_4)\cdot 2H_2O$ precursor has been obtained which is used to synthesize $LiFe_{0.4}Mn_{0.6-x}Ni_xPO_4$. With the increase of doping Ni content, $LiFe_{0.4}Mn_{0.6-x}Ni_xPO_4$/C exhibits improved performance including rate capability and cycling stability. Among the investigated samples, $LiFe_{0.4}Mn_{0.55}Ni_{0.05}PO_4$ shows the best electrochemical performance with 142 mAh g^{-1} at 0.1 *C*, and remains 110 mAh g^{-1} at 2 *C*. The improved rate ability is attributed to that the doping Ni^{2+} causes defects, which accelerates Li^+ movement in the crystal and alleviates polarity of the electrode reaction of the phosphate solid solution.

References

1. Padhi AK, Nanjundaswamy KS, Goodenough JB (1997) J Electrochem Soc 144:1188
2. Delacourt C, Wurm C, Reale P, Morcrette M, Masquelier C (2004) Solid State Ionics 173:113
3. Delacourt C, Laffont L, Bouchet R, Wurm C, Leriche JB, Morcrette M, Tarascon JM, Masquelier C (2005) J Electrochem Soc 152:A913
4. Choi D, Wang D, Bae IT, Xiao J, Nie Z, Wang W, Viswanathan VV, Lee YJ, Zhang JG, Graff GL, Yang Z, Liu J (2010) Nano Lett 10:2799
5. Xiao J, Xu W, Choi D, Zhang J (2010) J Electrochem Soc 157:A142
6. Yonemura M, Yamada A, Takei Y, Sonoyama N, Kanno R (2004) J Electrochem Soc 151:A1352
7. Li G, Azuma H, Tohda M (2002) J Electrochem Soc 149:A743
8. Yamada A, Kudo Y, Liu KY (2001) J Electrochem Soc 148:A747
9. Yamada A, Kudo Y, Liu KY (2001) J Electrochem Soc 148: A1153
10. Yamada A, Chung SC (2001) J Electrochem Soc 148:A960
11. Martha SK, Grinblat J, Haik O, Zinigrad E, Drezen T, Miners JH, Exnar I, Kay A, Markovsky B, Aurbach D (2009) J Angew Chem Int 48:8559
12. Hu CL, Yi HH, Fang HS, Yang B, Yao YC, Ma WH, Dai YN (2010) Electrochem Commun 12:1784
13. Mi CH, Zhang XG, Zhao XB (2006) Mater Sci Eng B 129:8
14. Qin HQ, Tao ZZ (2007) Battery Bimonthly 37:38
15. Xie H, Zhou ZT (2006) J Inorgan Mater 21:591
16. Tarascon JM, Wang E, Shokoohi FK, McKinnon WR, Colson S (1991) J Electrochem Soc 138:2859
17. Lee KS, Myung ST, Bang HJ, Chung S, Sun YK (2007) Electrochim Acta 52:5201
18. Wang C, Lu S, Kan S, Pang J, Jin W, Zhang X (2009) J Power Sour 189:607
19. Amarilla JM, Petrov K, Picó F, Avdeev G, Rojo JM, Rojas RM (2009) J Power Sour 191:591
20. Hua LG, Ikuto H, Uchida T, Wakihara M (1996) J Electrochem Soc 143:178
21. Liu W, Farrington GC, Chaput F, Dunn B (1996) J Electrochem Soc 143:879
22. Lee JH, Hong JK, Jang DH, Sun YK, Oh SM (2000) J Power Sour 89:7
23. Zhang Y, Sun CS, Zhou Z (2009) Electrochem Commun 11:1183
24. Howard WF, Spotnitz RM (2007) J Power Sour 165:887
25. Kang SH, Thackeray MM (2009) Electrochem Commun 11:748
26. Angermann A, Topfer J (2008) J Mater Sci 43:5123
27. Abrahams I, Easson KS (1993) Acta Cryst C 49:925
28. Deniard P, Dulac AM, Rocquefelte X, Grigorova V, Lebacq O, Pasturel A, Jobic S (2004) J Phys Chem Solids 65:229
29. Zhou F, Cococcioni M, Kang K, Cedar G (2004) Electrochem Commun 6:1144